annalen der physik
www.ann-phys.org

Calibration of the Solid-State Nuclear Magnetic Resonance Search for Axion-Like Dark Matter

Andrew J. Winter, Tanja Marić, Viktoriya A. Balabanova, János Ádám, Glenn Randall, Arne Wickenbrock, Derek F. Jackson Kimball, Dmitry Budker, and Alexander O. Sushkov**

Calibration of nuclear-magnetic-resonance-based searches for axion-like dark matter can be performed by free induction decay (FID) measurements. This manu- script describes FID experiments on several solid materials, motivated by the Cosmic Axion Spin Precession Experiment (CASPEr) program. Experiments with ^{207}Pb nuclear spins in ferroelectrics, lead magnesium niobate-lead titanate $(PbMg_{1/3}Nb_{2/3}O_3)_{2/3}-(PbTiO_3)_{1/3}$ (PMN-PT) and lead zirconium titante $PbZr_{0.52}Ti_{0.48}O_3$ (PZT) are directly relevant to the CASPEr-electric search for the electric dipole moment interaction of axion-like dark matter. Experiments with ^{31}P nuclear spins in gadolinium-doped hydroxypyromorphite $Pb_{4.95}Gd_{0.05}(PO_4)_3OH$ (HPM:Gd) are used for apparatus calibration. The measurements characterized the nuclear spin ensemble coherence time and the magnetic resonance detection sensitivity for these samples. Calibration is performed using small tip-angle pulses.

1. Introduction

Cosmological observations imply the existence of dark matter, which cannot be one of the Standard Model particles. However, despite decades of experimental searches, none of its non-gravitational interactions have been detected.[1–4] High energy physics models, such as grand unified theories and models with extra dimensions, incorporate light pseudoscalar bosons (axion-like particles, ALPs), which are potential dark matter candidates.[5–9] The ALP mass is unknown, but can be within the range of approximately 10^{-21}eV to 10^{-3}eV.[10–12] The strong CP problem of quantum chromodynamics (QCD) is resolved by the QCD axion, making it of particular interest.[9,13–16] The Cosmic Axion Spin Precession Experiment-electric (CASPEr-e) is a solid-state nuclear magnetic resonance (NMR) experiment designed to detect the interaction of ALP dark matter with a polarized ferroelectric sample. The EDM or the gradient interaction of axion-like dark matter with nuclear spins creates an oscillating torque on them. The goal of CASPEr-e is to detect the resulting tilt of the nuclear spins, by inductively coupling the sample to a sensitive SQUID magnetometer. This tilt is maximized when the spin Larmor frequency is tuned to be resonant with the axion Compton frequency.[17,18] In order to quantify the sensitivity of the search to axion-like dark matter, it is necessary to carefully calibrate the apparatus. This is accomplished by NMR experiments in which radio frequency (RF) pulses are delivered to a sample, and the resulting free-induction decay (FID) detected by an inductively-coupled current sensor. Reference [18] contains the description of the experimental details. The purpose of the calibration NMR experiments, described in the present work, is to characterize the NMR properties of the nuclear spin ensemble and measure the transfer function of the NMR detection circuit, in preparation for the ALP search.

2. Results and Discussion

The following materials were examined: lead magnesium niobate-lead titanate $(PbMg_{1/3}Nb_{2/3}O_3)_{2/3}-(PbTiO_3)_{1/3}$ (PMN-PT), lead zirconium titante $PbZr_{0.52}Ti_{0.48}O_3$ (PZT), and gadolinium-doped hydroxypyromorphite $Pb_{4.95}Gd_{0.05}(PO_4)_3OH$ (HPM:Gd). The first two listed samples are relevant in the CASPEr-e search for the electric dipole moment interaction

A. J. Winter, T. Marić, J. Ádám, G. Randall, A. O. Sushkov
Department of Physics
Boston University
Boston, MA 02215, USA
E-mail: ajwint@bu.edu; asu@bu.edu

V. A. Balabanova
Department of Physics
University of Massachusetts Dartmouth
North Dartmouth, MA 02747, USA

A. Wickenbrock, D. Budker
Johannes Gutenberg-Universität Mainz
55128 Mainz, Germany

A. Wickenbrock, D. Budker
Helmholtz-Institut
GSI Helmholtzzentrum für Schwerionenforschung
55128 Mainz, Germany

A. O. Sushkov
Department of Electrical and Computer Engineering
Boston University
Boston, MA 02215, USA

D. F. Jackson Kimball, D. Budker
Department of Physics
California State University – East Bay
Hayward, California 94542-3084, USA

A. O. Sushkov
Photonics Center
Boston University
Boston, MA 02215, USA

The ORCID identification number(s) for the author(s) of this article can be found under https://doi.org/10.1002/andp.202300252

DOI: 10.1002/andp.202300252

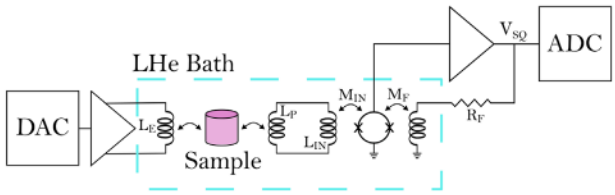

Figure 1. CASPEr-e circuit diagram. Beginning at the digital-to-analog converter (DAC) on the left, an analog RF signal is produced at room temperature and sent to the experiment in the LHe bath. The sample cylinder lies in a Helmholtz coil L_E and thus obtains some transverse magnetization. The sample also lies within a pickup coil gradiometer L_P perpendicular to L_E and external longitudinal field B_0. As the nuclear spins precess, a decaying sinusoidal signal is induced in L_P. The signal is then transferred from the SQUID input coil L_{in} to the flux-locked loop (FLL) with a mutual inductance of M_{in}. The FLL locks a to a quantized magnetic flux and is a part of a negative feedback loop, where R_F is the feedback resistance. R_F is in series with an inductor with mutual inductance M_F with the FLL. This produces a voltage signal V_{SQ}, which is then measured by the analog-to-digital converter (ADC) at room temperature.

of ALP dark matter. ^{31}P is present in HPM:Gd and has 100% natural abundance, which is much greater than the 22.1% abundance of ^{207}Pb. The gyromagnetic ratio of ^{31}P is approximately twice that of ^{207}Pb.[19,20] This makes it suitable for calibrating the experimental apparatus, because it is desirable for samples to have a high natural abundance for the nuclei of interest. High natural abundance provides a larger ensemble of nuclear spins that can be addressed in the NMR experiments, increasing the signal-to-noise ratio (SNR). The spin coherence time T_2^* for ^{31}P NMR in a material with similar structure (hydroxyapatite, HAp, which HPM:Gd was based on) has been measured to be on the order of ≈100 μs.[21] The HPM:Gd sample was doped with Gd so that the spin-lattice time T_1 would be decreased as a result of dipole–dipole interactions between the nuclei of interest and the Gd electron spins.[22] This allows optimization of the duty cycle of the NMR experiments. Simultaneously, HPM:Gd allows the opportunity to measure both ^{31}P and ^{1}H NMR.

The HPM:Gd sample was synthesized using the following reaction in aqueous solution:

$$\begin{aligned} 4.95Pb(NO_3)_2 + 0.05Gd(NO_3)_3 \cdot 6H_2O + 3(NH_4)_2HPO_4 \\ +6.75H_2O \rightarrow Pb_{4.95}Gd_{0.05}(PO_4)_3OH \\ +6NH_4OH + 10.05HNO_3 + 0.05OH^- \end{aligned} \quad (1)$$

This follows the procedure described in ref. [22]. The lead nitrate was obtained from Alfa Aesar with 99% purity, and the remaining two reactants were obtained from Sigma–Aldrich, with specified purities of 99.9% for the gadolinium nitrate hexahydrate and ≥98% for the ammonium phosphate. After dissolving under stirring, solutions were added to a teflon-lined pressure reactor and heated to 130°C for 18 h. The precipitate was extracted by using a centrifuge and heated to 70°C to evaporate excess water and produce the final HPM:Gd sample.

The NMR FID experiment begins with a radio frequency (RF) pulse of length τ, synthesized with the Spectrum Instrumentation digital-to-analog converter (DAC) card, amplified, and delivered to a 17-turn Helmholtz excitation coil, Figure 1. The pulse tilts the initially z-oriented sample spins toward the xy-plane by angle θ. After the pulse ends, the transverse spin projection precesses at the Larmor frequency and decays with relaxation time T_2^*. The oscillating magnetization induces a voltage in the pick-up coil with inductance L_p, wound in the second-order-gradiometer configuration, and orthogonal to the axis of the excitation coil. The NbTi pickup coil is connected to the input terminals of a Magnicon superconducting quantum interference device (SQUID). The SQUID is operated in the flux-locked loop (FLL) mode, converting the magnetic flux in the pickup coil to voltage, which becomes the output signal of the experiment. The detector transfer function is defined as

$$\alpha = \frac{V_{SQ}}{\mu_0 M_1} \quad (2)$$

where V_{SQ} is the FID signal SQUID output voltage, μ_0 is the permeability of free space, and M_1 is the transverse magnetization of the sample, discussed below. The SQUID parameters for these experiments were as follows: feedback resistance $R_f = 7$ kΩ and gain bandwidth product GBP = 7.2 GHz for PMN-PT, $R_f =$ 10 kΩ, GBP = 7.2 GHz for HPM:Gd, and $R_f = 30$ kΩ, GBP = 5 GHz for PZT. The SQUID output voltage was amplified by an SRS SR445a 5× preamplifier before being digitized. The SQUID noise spectrum contains audio-frequency vibrational peaks, but above ≈ 10kHz the noise is approximately white, at the level of 1.3 $\mu\Phi_0/\sqrt{\text{Hz}}$ (referred to the SQUID). Using the pickup circuit transfer function, we calculate the corresponding sensitivity to the magnetic field created by the sample ≈ 17fT/$\sqrt{\text{Hz}}$. The SQUID white noise is the dominant source of noise in the NMR measurements described in this work.

The magnetic resonance condition is that the excitation pulse carrier frequency is near the Larmor frequency $\omega_L = \gamma_n B_0$, where γ_n is the nuclear gyromagnetic ratio and B_0 is the bias magnetic field created by the solenoid magnet. The magnet coil constant β relates the current I in the magnet to B_0:

$$\beta = B_0/I \quad (3)$$

NMR measurements were used for magnetic field calibration to determine β, as described below.

Once the FID in time-domain has been recorded, the Fourier transform of the FID signal is taken to convert the data to the frequency domain. The FID signal lineshape is modeled as a Lorentzian with the absorptive and dispersive quadratures given by:

$$\Lambda_{abs} = \frac{A}{\sqrt{2t_D}} \frac{\Gamma}{\Gamma^2 + (2\pi(f_0 - f))^2} \quad (4)$$

$$\Lambda_{disp} = \frac{A}{\sqrt{2t_D}} \frac{2\pi(f - f_0)}{\Gamma^2 + (2\pi(f_0 - f))^2} \quad (5)$$

where f is the frequency, A is the fit amplitude, t_D is the time duration of the window that the Fourier transform is taken over, Γ is the fit linewidth, and f_0 is the fit center frequency. The coherence time can be extracted from the full width at half max (FWHM):

$$\text{FWHM} = \frac{\Gamma}{\pi} = \frac{1}{\pi T_2^*} \quad (6)$$

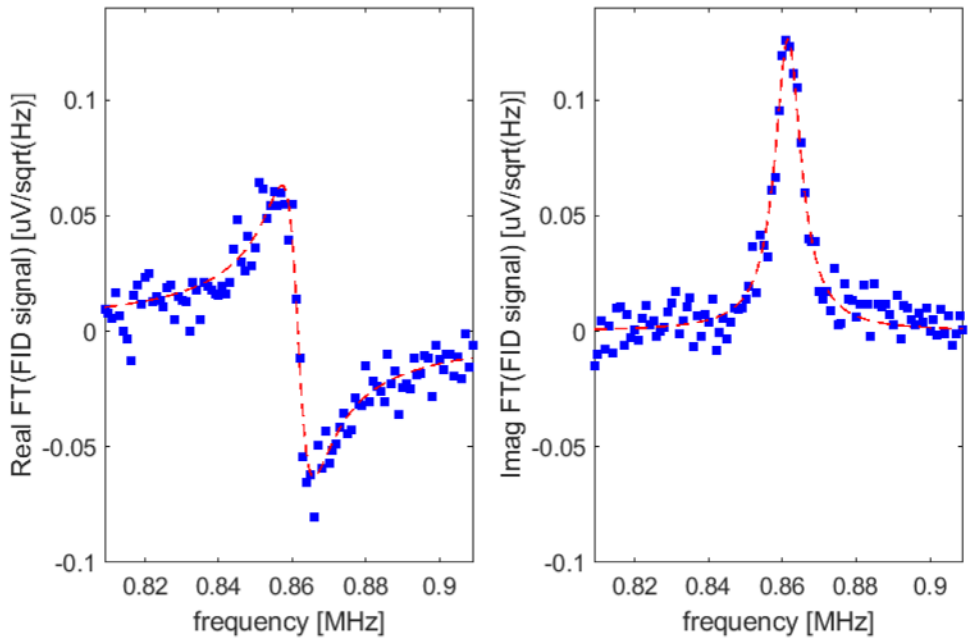

Figure 2. Fourier transform (FT) of HPM:Gd ^{31}P FID signal, which is centered at 862 kHz, from an excitation pulse of 894 kHz and a 60 μs pulse duration. The data are an average of 10000 measurements.

The fits to the ^{31}P FID data taken with the HPM:Gd sample at the Larmor frequency near 860 kHz are shown in Figure 2. The fits to the ^{207}Pb FID data taken with the PMN-PT sample at the Larmor frequency near 5.28 MHz are shown in Figure 3. The fits to the ^{207}Pb FID data taken with the PZT sample at the Larmor frequency near 4.6 MHz are shown in Figure 4. The sample properties and best-fit parameters are listed in Tables 1 and 2 respectively. The listed values of $1/T_2^*$ are extracted from the fitted linewidth using Equation (6).

The fitting was performed simultaneously for both signal quadratures. To obtain purely absorptive and dispersive quadratures, the fitted phase was used to appropriately shift the Fourier transform phase. In order to obtain best-fit parameter uncertainties, the bootstrapping approach was used. The

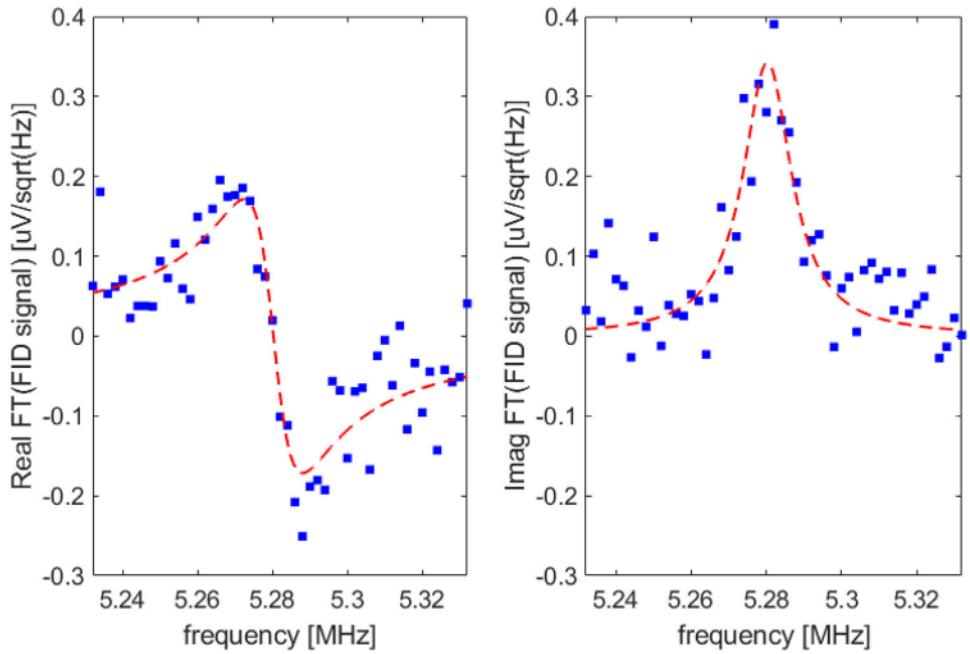

Figure 3. Fourier transform (FT) of PMN-PT ^{207}Pb FID signal in frequency domain centered at 5.28 MHz from an excitation pulse at 5.28 MHz and a 40 μs pulse duration. The data are an average of 1000 measurements.

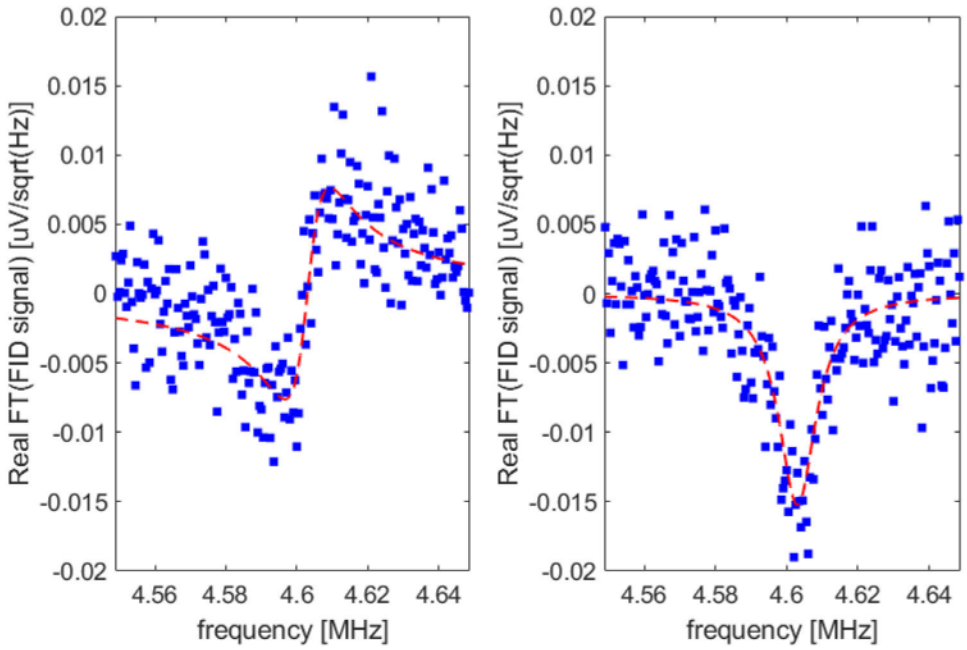

Figure 4. Fourier transform (FT) of PZT ^{207}Pb FID signal in frequency domain centered at 4.6 MHz, from an excitation pulse of 4.6 MHz and a 20 μs pulse duration. The data are an average of 10000 measurements.

Table 1. Sample properties.

Sample (isotope)	Natural abundance	γ_n (rads s^{-1}T^{-1})	Diameter (cm)	Length (cm)	Spin I
PMN-PT (^{207}Pb)	22.1% [20]	5.581×10^7 [20]	0.46	0.50	1/2
PZT (^{207}Pb)	22.1%	5.581×10^7	0.45	0.50	1/2
HPM:Gd (^{31}P)	100% [19]	10.832×10^7 [19]	0.40	0.6*	1/2

*The HPM:Gd powder sample was tightly packed into a gelatin capsule, with a mica cap placed on top then sealed shut with cryogenic epoxy.

Fourier-transformed data were decimated into thirds, to build three datasets.

Undersampling by a factor of three still maintained at least 5-6 points across the linewidth, which was sufficient to fit the Lorentzian lineshape. The three datasets were then fitted with Lorentzian lineshapes, and the standard deviation of each fit parameter was used as the uncertainty.

For each of the three samples the FID data were recorded at several values of the magnet current, **Figure 5**. A linear fit was performed on each data set and the best-fit slope is listed in Table 2. The data sets were then combined by dividing each FID frequency value by the corresponding gyromagnetic ratio, **Figure 6**. When a linear fit was performed on these data, the resulting slope corresponds to the magnet coil constant: $\beta = (1416.6 \pm 0.3) \times 10^{-4}$ T/A. This is consistent with magnet's specification of 1407×10^{-4} T/A. The uncertainty corresponds to the one standard deviation confidence interval of the fit.

Table 2. Measurements for ^{207}Pb NMR in PMN-PT and PZT, and ^{31}P NMR in HPM:Gd, and calculated magnet constant for each sample.

Sample (NMR)	$1/T_2^*$ (ms^{-1})	f_0 (kHz)	A (μV)	β ($\times 10^{-4}$ T/A)
PMN-PT (Pb)	47 ± 6	5280 ± 1	0.54 ± 0.06	1416.8 ± 0.1
PZT (Pb)	39 ± 2	4603.1 ± 0.7	0.038 ± 0.001	1416.2 ± 1.0
HPM:Gd (P)	27 ± 1	862 ± 0.2	0.150 ± 0.008	1399 ± 9

Under equilibrium conditions, the spin ensemble magnetization is oriented along the bias magnetic field, and has the value of

$$\mu_0 M_0 = \mu_0 \frac{n\gamma_n^2 \hbar^2 I(I+1) B_0}{3k_B T} \tag{7}$$

where n is the number density of nuclear spins, γ_n is the gyromagnetic ratio for the nuclear species, and B_0 is the external magnetic field.[18] With an external magnetic field of 0.59 T, the PMN-PT ^{207}Pb spin ensemble magnetization is ≈370 pT, and with 0.52 T the PZT spin ensemble magnetization is ≈340 pT.

After a single resonant RF excitation pulse of length τ the nuclear spins are tilted by angle $\theta = \Omega_e \tau$, where Ω_e is the Rabi frequency. This creates the transverse magnetization

$$\mu_0 M_1 = \mu_0 M_0 \sin\theta = \mu_0 M_0 \sin\left(\Omega_e \tau\right) \approx \mu_0 M_0 \Omega_e \tau \tag{8}$$

where the last approximation is valid for $\theta \ll 1$. The FID is recorded after the pulse, and the transverse magnetization decays on the time scale T_2^*. In order to calibrate the transfer function α, an independent measurement of the transverse magnetization

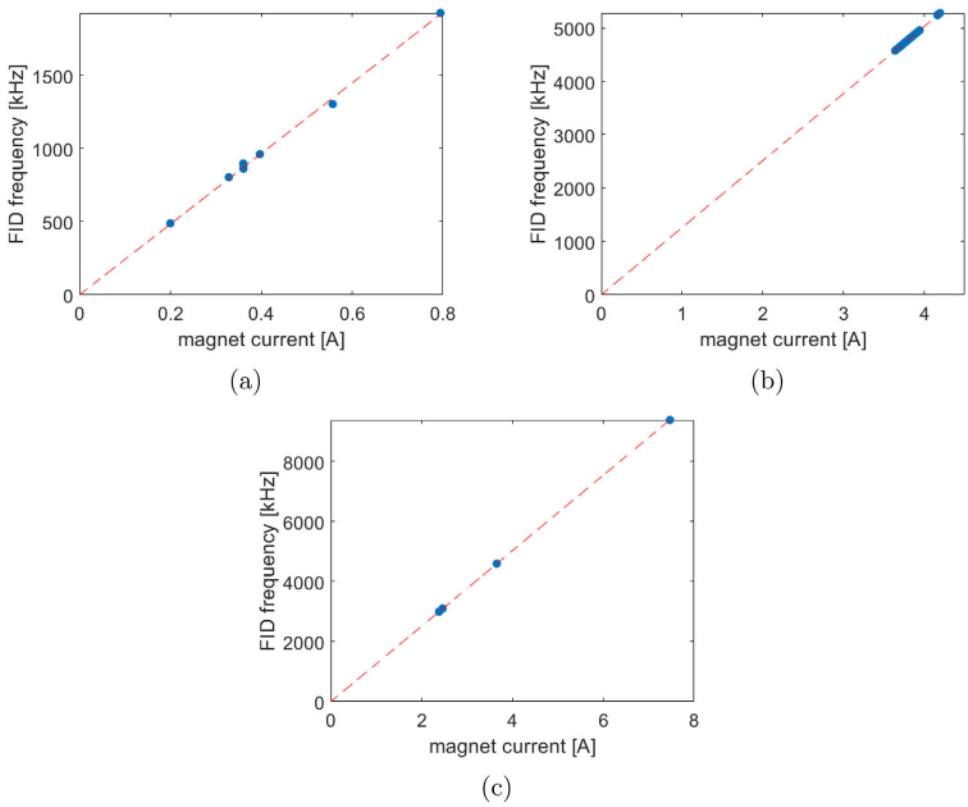

Figure 5. a) HPM:Gd ^{31}P, b) PMN-PT's ^{207}Pb, and c) PZT's ^{207}Pb FID frequencies varying with equilibrium magnetic field B_0.

is needed. This is achieved by delivering a sequence of N excitation pulses. Since only the z-projection of the spin magnetization survives after each pulse, the FID amplitude scales as

$$A(N) = A_0(\cos\theta)^N + c \tag{9}$$

This describes spin saturation, and the constant c accounts for incomplete saturation due to the relaxation back towards thermal equilibrium, Equation (7). The fit of the FID amplitude as a function of pulse number was used to extract the tilting angle $\theta = (0.085 \pm 0.004)$ rad for PMN-PT, **Figure 7**. Using this tilting angle, the transfer function was calculated to be $\alpha = (1.2 \pm 0.2) \times 10^7$ V/T, consistent with ref. [23]. The uncertainty was obtained by collecting multiple sets of data and using the standard

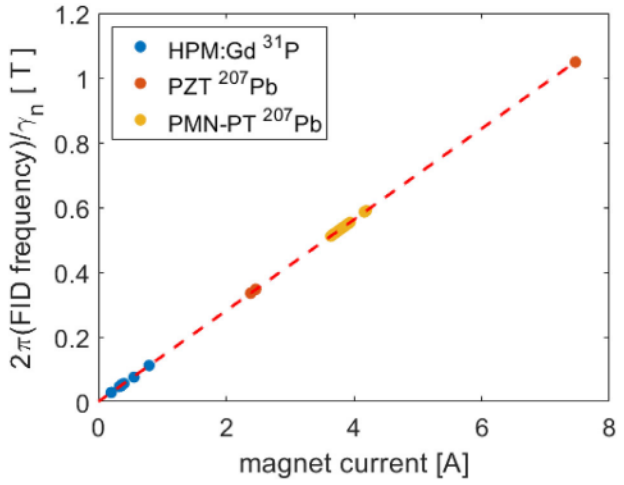

Figure 6. All of the samples' FID frequencies converted to angular frequency, then divided by their respective nuclear gyromagnetic ratios plotted against magnet current. The slope of the fitted line is $(1416.6 \pm 0.3) \times 10^{-4}$ T/A.

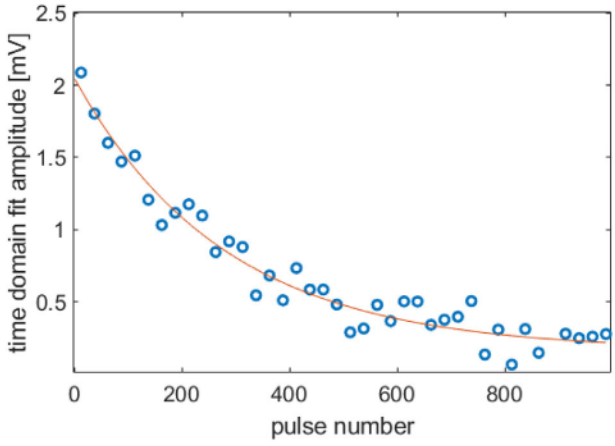

Figure 7. Example PMN-PT tilting angle fit with a 40 μs pulse length at 5282 kHz and 2.2 ms in between each successive pulse. This particular fit resulted in $A_0 = (1.9 \pm 0.1)$ mV and $\theta = (0.085 \pm 0.004)$ rad.

deviation of the results. In order to verify that the signals observed in the experiments were indeed due to the nuclear spins in the samples (rather than, for example, SQUID response oscillations), a series of background experiments were performed. When the carrier frequency of the excitation pulse was set to be far detuned from the nuclear Larmor frequency, no FID was observed. In addition, changing the bias magnetic field shifted the FID frequency consistently with the correct nuclear spin gyromagnetic ratio (Figure 5).

3. Conclusion

This manuscript describes experiments that calibrate the parameters of the CASPEr-e solid-state NMR search for axion-like dark matter. These calibrations are important for choosing the optimal sample and interpreting the axion-search data. The unique challenge of these cryogenic solid-state NMR experiments is the absence of sample magic-angle spinning or other line-narrowing approaches, which necessitates working with short nuclear spin coherence times, due to inhomogeneous and dipolar relaxation. This degrades the NMR signal-to-noise ratio. Despite this challenge, sensitive SQUID detection allowed FID measurements described in the present work. Because of the short spin coherence time, a $\pi/2$ tipping pulse was not feasible in the experimental setup, which emphasized detection sensitivity over excitation amplifier power. Nevertheless, the SQUID detection sensitivity allowed FID detection with small tip angle pulses, combined with averaging of many FID experiments. Using a small tip angle excitation reduces the FID amplitude, but it also preserves a large fraction of longitudinal spin polarization, after the FID decays. This allows multiple averages of the FID experiment, and, in the end, the SNR is comparable to what could be achieved with a single $\pi/2$ pulse FID. Thus, it is shown that the calibration of a solid-state NMR search for axion-like dark matter can be performed without having to apply $\pi/2$ tip angle pulses.

Acknowledgements

This work was supported by the National Science Foundation CAREER grant PHY-2145162, and the U.S. Department of Energy, Office of High Energy Physics program under the QuantISED program, FWP 100667. V. A. B. was supported by the NSF REU grant 1852266. A.W. and D.B. acknowledged support by the Cluster of Excellence "Precision Physics, Fundamental Interactions, and Structure of Matter" (PRISMA+ EXC 2118/1) and by COST (European Cooperation in Science and Technology). D.F.J.K. acknowledged support from the U.S. National Science Foundation under grant PHY-2110388.

Conflict of Interest

The authors declare no conflict of interest.

Data Availability Statement

The data that support the findings of this study are available from the corresponding author upon reasonable request.

Keywords

axions, dark matter, solid state nuclear magnetic resonance

Received: May 31, 2023
Revised: August 28, 2023
Published online:

[1] D. N. Spergel, *Science* **2015**, *347*, 1100.
[2] G. Bertone, T. M. P. Tait, *Nature* **2018**, *562*, 51.
[3] A. Arbey, F. Mahmoudi, *Prog. Part. Nucl. Phys.* **2021**, *119*, 103865.
[4] D. F. Jackson Kimball, L. D. Duffy, D. J. E. Marsh, Ultralight Bosonic Dark Matter Theory. *The Search for Ultralight Bosonic Dark Matter*, Eds., D. F. Jackson Kimball, K. van Bibber, Springer International Publishing, Cham **2023**.
[5] J. Preskill, M. B. Wise, F. Wilczek, *Phys. Lett. B* **1983**, *120*, 127.
[6] L. F. Abbott, P. Sikivie, *Phys. Lett. B* **1983**, *120*, 133.
[7] M. Dine, W. Fischler, *Phys. Lett. B* **1983**, *120*, 137.
[8] P. Svrcek, E. Witten, *J. High Energy Phys* **2006**, *2006*, 51.
[9] I. G. Irastorza, J. Redondo, *Prog. Part. Nucl. Phys.* **2018**, *102*, 89.
[10] P. W. Graham, A. Scherlis, *Phys. Rev. D* **2018**, *98*, 035017.
[11] A. Ernst, A. Ringwald, C. Tamarit, *J. High Energy Phys.* **2018**, *2018*, 103.
[12] K. Schutz, *Phys. Rev. D* **2020**, *101*, 123026.
[13] R. D. Peccei, H. R. Quinn, *Phys. Rev. Lett.* **1977**, *38*, 1440.
[14] S. Weinberg, *Phys. Rev. Lett.* **1978**, *40*, 223.
[15] F. Wilczek, *Phys. Rev. Lett.* **1978**, *40*, 279.
[16] D. DeMille, J. M. Doyle, A. O. Sushkov, *Science* **2017**, *357*, 990.
[17] D. Budker, P. W. Graham, M. Ledbetter, S. Rajendran, A. O. Sushkov, *Phys. Rev. X* **2014**, *4*, 21030.
[18] D. Aybas, J. Adam, E. Blumenthal, A. V. Gramolin, D. Johnson, A. Kleyheeg, S. Afach, J. W. Blanchard, G. P. Centers, A. Garcon, M. Engler, N. L. Figueroa, M. Gil Sendra, A. Wickenbrock, M. Lawson, T. Wang, T. Wu, H. Luo, H. Mani, P. Mauskopf, P. W. Graham, S. Rajendran, D. F. Jackson Kimball, D. Budker, A. O. Sushkov, *Phys. Rev. Lett.* **2021**, *126*, 141802.
[19] M. Stovell, J.-L. Yan, A. Sleigh, M. Mada, T. Carpenter, P. J. Hutchinson, K. L. Carpenter, *Front. Neurol.* **2017**, *8*, https://doi.org/10.3389/fneur.2017.00426
[20] E. Kirstein, D. R. Yakovlev, M. M. Glazov, E. Evers, E. A. Zhukov, V. V. Belykh, N. E. Kopteva, D. Kudlacik, O. Nazarenko, D. N. Dirin, M. V. Kovalenko, M. Bayer, *Adv. Mater.* **2022**, *34*, 2105263.
[21] Y. Wu, J. L. Ackerman, H. M. Kim, C. Rey, A. Barroug, M. J. Glimcher, *J. Bone Miner. Res.* **2002**, *17*, 472.
[22] N. L. Ignjatović, L. Mancić, M. Vuković, Z. Stojanović, M. G. Nikolić, S. Škapin, S. Jovanovic, L. Veselinovic, V. Uskokovic, S. Lazic, S. Markovic, M. M. Lazarevic, D. P. Uskokovic, *Sci. Rep.* **2019**, *9*, 1.
[23] Manuscript in preparation.

